

The reaction $^{13}\text{C}(\alpha, n)^{16}\text{O}$: a background for the observation of geo-neutrinos

S. Harissopulos¹, H. W. Becker², J. W. Hammer³, A. Lagoyannis¹, C. Rolfs⁴, F. Strieder⁴

¹*Institute of Nuclear Physics, NCSR “Demokritos”,*

153.10 Aghia Paraskevi, Athens, Greece

²*Dynamitron-Tandem-Laboratorium,*

Ruhr-Universität Bochum, 44801 Bochum, Germany

³*Institut für Strahlenphysik, Universität Stuttgart, 70569 Stuttgart, Germany and*

⁴*Institut für Physik mit Ionenstrahlen,*

Ruhr-Universität Bochum, 44801 Bochum, Germany

(Dated: June 10, 2018)

Abstract

The absolute cross section of the $^{13}\text{C}(\alpha, n)^{16}\text{O}$ reaction has been measured at $E_\alpha = 0.8$ to 8.0 MeV with an overall accuracy of 4%. The precision is needed to subtract reliably a background in the observation of geo-neutrinos, e.g. in the KamLAND detector.

PACS numbers: 25.40.Ny, 26., 27.20.+n

I. INTRODUCTION

In order to understand better the energy source of the earth, e.g. the radioactive decay of U, Th and others, the KamLAND neutrino detector is planning to observe the geo-neutrinos from these decays. The antineutrinos ν_a from the decays in the earth interact with the protons in the liquid scintillator of KamLAND via the inverse β decay $\nu_a + p \rightarrow n + e^+$ and are detected with phototubes via the combination of (i) a prompt signal from the slowing down and annihilation of the e^+ and (ii) a delayed signal provided by the 2 MeV γ -ray from the $p(n,\gamma)d$ reaction, which occurs after the neutron has been thermalized.

The KamLAND detector consists of 1 kilotons of organic scintillator and contains thus about 10 tons of ^{13}C . The detector contains also 10^{-20} g/g of ^{210}Pb nuclides (half-life = 22.3 y), which decay via ^{210}Bi and ^{210}Po into ^{206}Pb emitting in the process a 5.3 MeV α -particle. When these α -particles slow down in the scintillator, they can initiate the $^{13}\text{C}(\alpha,n)^{16}\text{O}$ reaction ($Q = 2.215$ MeV), whereby the fast neutrons perfectly mimic the antineutrino signal. Firstly, the few MeV neutron transfers its kinetic energy to the protons in the medium, such that a few MeV proton emerges from this first collision. The proton in turn produces ionisation, which results in a prompt signal simulating (i). A prompt signal (i) can also be created in the slowing down (ionization) of the 5.3 MeV alpha-particle. Secondly, as the neutron is slowed down it will create a signal like (ii). In this way a fake antineutrino signal is built.

The $^{13}\text{C}(\alpha,n)^{16}\text{O}$ reaction creates an important background and gives a number of fake events which are comparable to those expected from geo-neutrinos [?]. For detecting geo-neutrinos one needs to subtract the fake events in a reliable way. With the present 30% uncertainty in the absolute cross section σ of $^{13}\text{C}(\alpha,n)^{16}\text{O}$ over the relevant energy range (measured in [?] at $E_\alpha = 1.0$ to 5.4 MeV), it appears impossible [?] to extract a geo-neutrino signal from any detector at any place in the world. Calculations indicate [?] that for a 10% uncertainty in σ the discovery of geo-neutrinos will be achievable. In recent years new precise σ measurements have been carried out at low energies [? ?], i.e. below $E_\alpha = 1.1$ MeV. We report on new precise σ measurements in the energy range $E_\alpha = 0.8$ to 8.0 MeV.

II. EQUIPMENT AND PROCEDURES

The tandem accelerator of the Dynamitron - Tandem - Laboratorium (DTL) at the Ruhr-Universität Bochum provided the ^4He beam, with a current on target of less than 100 nA. The absolute energy of the beam was checked to a precision of ± 3 keV; the energy spread was 0.8 keV at $E_\alpha = 1.0$ MeV. The beam passed through collimators of $\varnothing = 15, 3,$ and 5 mm diameter at a distance from the target of 3.06, 1.43, and 0.80 m, respectively, and was stopped at the target. The air-cooled target ($\varnothing = 40$ mm) was installed in an electrically insulated pipe of 0.80 m length ($\varnothing = 40$ mm), which served as a long Faraday cup. A suppression voltage of 300 V was applied to the last aperture in front of the target pipe and this led to a precision of 2% in the charge measurement at the target. The vacuum was better than 3×10^{-7} mbar.

The $22 \mu\text{g}/\text{cm}^2$ thick C target (on a 0.2 mm thick Ta backing) was enriched to 99% in ^{13}C . The enrichment was confirmed within $\pm 2\%$ using the narrow resonance at $E_{pr} = 1.748$ MeV in $^{13}\text{C}(p,\gamma)^{14}\text{N}$ (γ -ray detection with a 12×12 inch NaI crystal in close geometry, placed at another beam line) and comparing the thick-target γ -ray yields obtained for the above enriched target as well as for a C target of natural isotopic composition ($^{13}\text{C} = 1.1\%$). The results are shown in Fig. 1, where the enriched target was analysed at the completion of the $^{13}\text{C}(\alpha,n)^{16}\text{O}$ experiment: the 50% yield-point is identical for both targets indicating no detectable deposition of natural carbon on the enriched target. The deduced target thickness for the enriched target (Fig. 1) was $\Delta_p = 3.25 \pm 0.10$ keV, consistent with the value $\Delta_p = 3.14 \pm 0.10$ keV obtained initially. The results for the $E_{\alpha r} = 1.054$ and 1.336 MeV narrow resonances in $^{13}\text{C}(\alpha,n)^{16}\text{O}$ are shown in Fig. 2 leading to $\Delta_\alpha = 37.0 \pm 1.0$ and 33.2 ± 1.0 keV, respectively. Using stopping power tables [?] (with a 3% uncertainty [?]) one arrives at an average value for the ^{13}C areal target density of $N_t = (10.21 \pm 0.31) \times 10^{17}$ atoms/cm², where the quoted error arrives from the uncertainty in the stopping power.

The neutron yields were measured using a 4π detector consisting of thermal-neutron detectors, i.e. 16 ^3He -filled proportional counters (sensitive length = 45.7 cm, $\varnothing = 2.54$ cm, pressure = 4 bar), embedded in a polyethylene-cylinder moderator (length = 1.00 m, $\varnothing = 35.0$ cm) with a central bore hole ($\varnothing = 7.0$ cm) to install the target. At an inner circle of $\varnothing = 16.0$ cm there were 8 ^3He counters and at $\varnothing = 24.0$ cm there were another 8 ^3He counters, all embedded in holes of $\varnothing = 3.0$ cm in the moderator. The inner and outer counters

are positioned with a relative angle difference of 22.5° . To reduce the neutron background arising from cosmic showers, several components for passive shielding (Cd, polyethylene, bor-polyethylene, bor-paraffin) are placed around the moderator leading to a background rate of 0.22 counts/s. In the present experiment the spectra of the 16 counters were summed and stored in an ADC. To monitor dead time effects (kept below 4%), a pulser was used.

The neutron efficiency $\eta_n(E_n)$ as a function of neutron energy E_n (in MeV) was calculated with the Monte Carlo program MCNP leading to the expression [?]]

$$\eta_n(E_n) = 0.7904 + 0.1607(E_n + 247.07)\exp(-0.114E_n)[\%] \quad (1)$$

at $E_n = 2.0$ to 9.0 MeV. With a calibrated ($\pm 1.1\%$) ^{252}Cf source, the neutron detection efficiency at the mean energy $E_n = 2.3$ MeV was found [?]] to be $32.1 \pm 0.5\%$ in good agreement with the calculated value 31.6%. We used the calculated curve to correct the observed neutron yields for efficiency: over the energy range of the present experiment, $E_\alpha = 0.8$ to 8.0 MeV, $\eta_n(E_n)$ varies from 31% to 16% for a mean neutron emission angle of 90° .

III. RESULTS

An excitation function was obtained with the ^{13}C target at energies between $E_\alpha = 0.8$ and 8.0 MeV in steps of $\delta = 10$ keV, where the target thickness $\Delta(E_\alpha)$ varied between 39 and 13 keV, respectively. The exceptions in steps are for $E_\alpha > 7.2$ MeV ($\delta = 20$ keV) and near narrow resonances ($\delta = 0.2$ keV). The statistical error of each data point was better than 0.2%. After completion of the excitation function, yield tests were performed at selected energies over the total energy range leading to a reproducibility of better than 2% (=relative error).

For non-resonant energies, where the yields change slowly with energy, the observed yields (and thus the cross sections) are associated with an effective energy E_{eff} over the target thickness $\Delta(E_\alpha)$ [?]]. For energies with resonance structures, where the resonance width is comparable to the target thickness, the deduced value E_{eff} and associated yield represents a mean cross section over $\Delta(E_\alpha)$.

The observed neutron yield N_n at a given E_{eff} is related to the cross section $\sigma(E_{\text{eff}})$ via the relation [?]]

$$N_n = N_\alpha N_t \eta_n \sigma(E_{\text{eff}}) \quad (2)$$

where N_α is the number of incident α projectiles. At $E_{\text{eff}} = 1.00$ MeV we found $\sigma(E_{\text{eff}}) = 157 \pm 7 \mu\text{b}$, where the error corresponds to the quadratic sum of the uncertainties in N_n (1.6%), N_α (2.0%), N_t (3.0%) and η_n (1.7%). Our value is in good agreement with the previous value of $146 \pm 7 \mu\text{b}$ [?] leading to a weighted average of $152 \pm 5 \mu\text{b}$, which we adopted as reference value. With the relative error of 2% and this absolute error of 3% one arrives at an overall accuracy of 4% for the data of the present work.

For the case of the narrow resonances at $E_{\alpha r} = 1.054$ and 1.336 MeV (Fig. 2) and 1.590 MeV (not shown), the observed neutron yields lead to resonance strengths $\omega\gamma$, which represent the integral over the resonance width Γ : the respective widths are $\Gamma = 1.5, 0.6,$ and 1.0 keV [?] and the respective strengths are $\omega\gamma = 12.1 \pm 0.6, 33.3 \pm 1.8,$ and 11.5 ± 1.2 eV from the present work and $\omega\gamma = 11.9 \pm 0.6,$ not given, and 10.8 ± 0.5 eV from [?] leading to the accepted values of $\omega\gamma = 12.0 \pm 0.4, 33.3 \pm 1.8,$ and 10.9 ± 0.5 eV. With these quantities we calculated the cross section $\sigma(E_{\alpha r})$ at the energy region of these resonances.

Our cross-section results plotted in Fig. 3 are also given in Table I. The present absolute cross sections for the non-resonant data are lower by about 30% compared to the values reported in previous work [?]: from the data shown in Fig. 3 of [?] we find $\sigma_{\text{present}}/\sigma_{[2]} \cong 0.63, 0.68, 0.64,$ and 0.72 at the broader resonances $E_\alpha = 2.3, 3.3, 4.4,$ and 5.0 MeV, respectively.

IV. CONCLUSIONS

With an overall accuracy of 4% for the absolute cross section of $^{13}\text{C}(\alpha, n)^{16}\text{O}$ one can subtract reliably this background in the KamLAND detector and thus the discovery of geo-neutrinos appears achievable.

Acknowledgments

This work supported in part by the German Academic Exchange Service (DAAD), the Hellenic State Scholarships Foundation (IKY), and the Dynamitron-Tandem-Laboratorium (DTL). The authors would like to thank G. Fiorentini for suggesting the experiment and J.

Wrachtrup for the loan of the neutron detector.

- G. Fiorentini, private communication (2004); T. Araki *et al.*, *Nature* 436, 499 (2005).
- J. K. Bair, F. X. Haas, *Phys. Rev. C* **7**, 1356 (1973).
- H. W. Drotleff, A. Denker, H. Knee, M. Soine, G. Wolf, J. W. Hammer, U. Greife, C. Rolfs, H. P. Trautvetter, *Ap. J.* **414**, 735 (1993).
- C. R. Brune, I. Licot, R. W. Kavanagh, *Phys. Rev. C* **48**, 3119 (1993).
- J. P. Biersack, J. F. Ziegler, *Transport of Ions in Matter, TRIM program version 2003* (IBM Research, New York, 1995)
- A. Denker, Ph.D thesis, Universität Stuttgart, (1994) unpublished.
- C. E. Rolfs, W. Rodney, *Cauldrons in the Cosmos* (The University of Chicago Press, Chicago 1986)

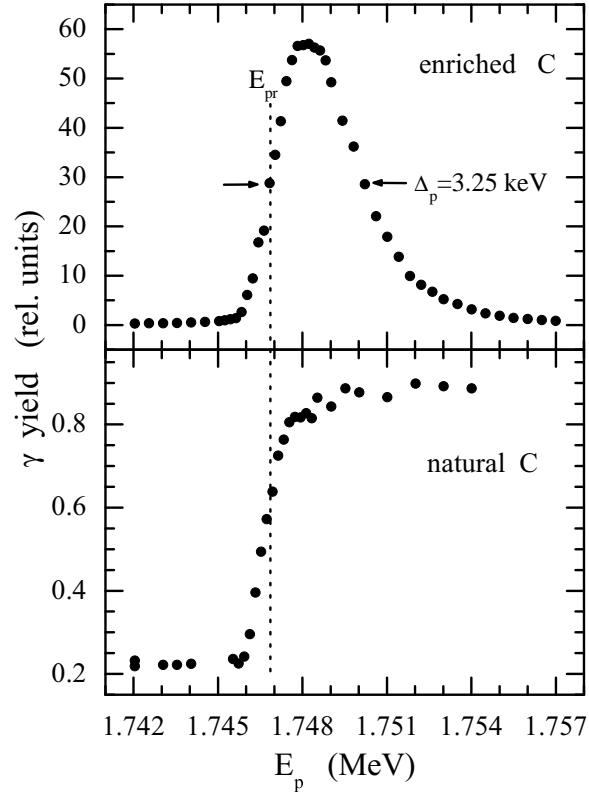


FIG. 1: Thick target γ -ray yield for the narrow $E_{pr} = 1.747$ MeV resonance in $^{13}\text{C}(p,\gamma)^{14}\text{N}$ obtained with a C target enriched in ^{13}C and with a C target of natural isotopic composition.

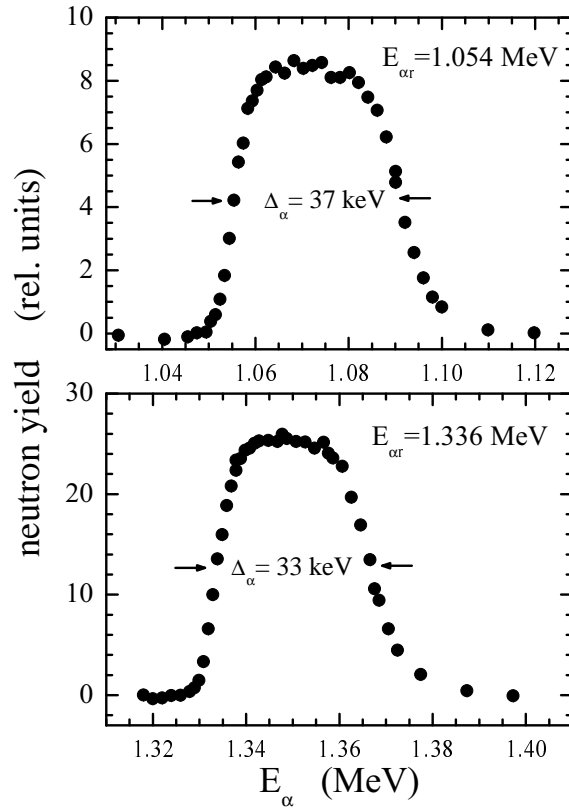


FIG. 2: Thick target neutron yield for the narrow $E_\alpha = 1.054$ and 1.336 MeV resonances in $^{13}\text{C}(\alpha, n)^{16}\text{O}$ obtained with a C target 99% enriched in ^{13}C ; and non-resonant yield has been subtracted from the data.

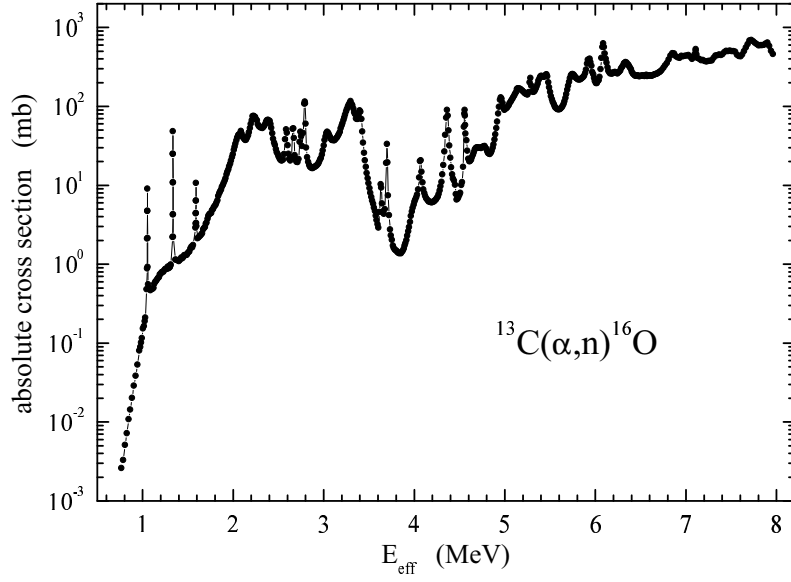


FIG. 3: Absolute cross section of $^{13}\text{C}(\alpha, n)^{16}\text{O}$ between $E_{\text{eff}} = 0.77$ and 7.96 MeV. The solid curve is to guide the eye only. For the narrow resonances at $E_{\alpha r} = 1.054$, 1.336 , and 1.590 MeV the corresponding resonant cross section was deduced from the measured strength and total width.

TABLE I: Absolute cross section of $^{13}\text{C}(\alpha,n)^{16}\text{O}$

E_{eff} (MeV)	σ (mb)	E_{eff} (MeV)	σ (mb)	E_{eff} (MeV)	σ (mb)	E_{eff} (MeV)	σ (mb)	E_{eff} (MeV)	σ (mb)	E_{eff} (MeV)	σ (mb)	E_{eff} (MeV)	σ (mb)	E_{eff} (MeV)	σ (mb)
0.767	0.0026	1.588	4.30	2.385	67.5	3.220	67.0	4.065	20.2	4.878	32.9	5.721	227	6.553	244
0.786	0.0033	1.589	6.25	2.395	66.1	3.230	72.1	4.074	20.7	4.888	37.8	5.731	247	6.563	250
0.807	0.0051	1.590	10.5	2.405	65.3	3.239	78.2	4.083	14.8	4.897	44.2	5.740	254	6.573	241
0.826	0.0072	1.591	6.26	2.414	59.8	3.249	85.8	4.092	10.9	4.907	53.0	5.750	256	6.583	243
0.846	0.0108	1.592	4.33	2.424	53.3	3.259	91.9	4.102	8.85	4.917	64.0	5.760	252	6.593	245
0.866	0.0143	1.593	3.32	2.434	45.6	3.269	99.0	4.113	7.96	4.927	80.7	5.770	245	6.603	246
0.886	0.0202	1.595	3.02	2.444	38.6	3.279	104	4.122	7.28	4.937	98.7	5.779	235	6.613	245
0.906	0.0287	1.609	2.12	2.454	34.5	3.289	110	4.132	6.81	4.947	121	5.789	228	6.623	243
0.925	0.0384	1.619	2.17	2.464	32.3	3.299	116	4.142	6.61	4.957	129	5.799	223	6.633	246
0.945	0.0532	1.629	2.23	2.473	28.6	3.309	107	4.152	6.37	4.967	124	5.809	219	6.643	250
0.965	0.0801	1.639	2.29	2.483	26.2	3.319	103	4.162	6.20	4.976	110	5.819	218	6.653	252
0.975	0.0893	1.649	2.38	2.493	24.7	3.329	93.4	4.172	6.19	4.986	95.8	5.829	219	6.662	254
0.985	0.101	1.660	2.45	2.503	23.1	3.338	84.1	4.183	6.10	4.996	90.2	5.839	220	6.672	259
0.994	0.116	1.670	2.75	2.513	21.7	3.348	79.7	4.193	6.03	5.006	92.4	5.850	224	6.682	258
1.005	0.152	1.680	2.85	2.524	21.0	3.358	69.9	4.203	6.07	5.016	93.1	5.860	230	6.692	264
1.016	0.164	1.690	2.95	2.534	20.5	3.368	68.9	4.213	6.17	5.026	95.6	5.870	236	6.702	268
1.025	0.189	1.699	3.24	2.544	20.7	3.378	68.8	4.223	6.23	5.036	99.0	5.880	244	6.712	273
1.030	0.209	1.709	3.34	2.554	21.1	3.388	76.4	4.232	6.43	5.046	103	5.889	265	6.722	279
1.046	0.461	1.719	3.73	2.565	24.7	3.399	88.6	4.242	6.59	5.056	109	5.899	291	6.732	287
1.050	0.850	1.730	4.11	2.576	38.3	3.409	85.6	4.252	6.86	5.066	114	5.909	346	6.752	307
1.052	2.03	1.740	4.30	2.586	51.1	3.418	68.8	4.262	7.15	5.076	119	5.919	389	6.771	329
1.053	4.53	1.749	4.37	2.595	46.2	3.427	48.0	4.272	7.70	5.086	124	5.929	389	6.791	353
1.054	8.77	1.759	4.42	2.602	32.1	3.436	34.7	4.282	8.55	5.096	131	5.939	366	6.811	392
1.055	4.54	1.769	4.81	2.611	24.9	3.446	25.7	4.292	9.70	5.106	137	5.939	401	6.831	438
1.056	2.04	1.779	4.98	2.621	21.5	3.457	20.7	4.302	11.0	5.115	144	5.948	363	6.851	469

Continued on next page

TABLE I: – continued from previous page

E_{eff}	σ	E_{eff}	σ	E_{eff}	σ	E_{eff}	σ	E_{eff}	σ	E_{eff}	σ	E_{eff}	σ	E_{eff}	σ
(MeV)	(mb)	(MeV)	(mb)	(MeV)	(mb)	(MeV)	(mb)	(MeV)	(mb)	(MeV)	(mb)	(MeV)	(mb)	(MeV)	(mb)
1.058	0.880	1.789	5.26	2.632	20.4	3.466	17.1	4.313	13.7	5.125	150	5.958	326	6.871	468
1.062	0.556	1.799	5.48	2.643	22.7	3.476	14.2	4.323	18.1	5.135	165	5.968	272	6.890	430
1.078	0.495	1.808	5.66	2.657	51.8	3.486	12.2	4.333	26.7	5.145	169	5.978	254	6.910	416
1.080	0.481	1.818	5.98	2.666	52.6	3.497	10.6	4.343	43.3	5.155	168	5.988	228	6.930	409
1.087	0.466	1.828	6.42	2.673	39.6	3.507	9.18	4.353	71.7	5.165	167	5.997	209	6.950	437
1.098	0.483	1.839	7.33	2.681	24.1	3.517	7.98	4.362	89.8	5.175	164	6.007	196	6.970	427
1.112	0.485	1.849	7.87	2.690	21.1	3.527	7.09	4.371	76.0	5.185	161	6.018	196	6.989	437
1.122	0.500	1.859	8.33	2.701	19.7	3.537	6.36	4.380	49.6	5.195	157	6.028	208	7.009	439
1.132	0.561	1.869	8.77	2.712	19.6	3.547	5.80	4.389	31.7	5.205	154	6.038	214	7.029	447
1.142	0.598	1.879	9.50	2.723	21.5	3.557	5.21	4.399	22.3	5.215	150	6.048	235	7.049	421
1.152	0.614	1.889	10.1	2.735	35.5	3.567	4.71	4.410	16.9	5.224	146	6.058	296	7.069	398
1.162	0.640	1.899	10.7	2.745	47.5	3.576	4.10	4.420	13.7	5.234	144	6.068	411	7.089	418
1.172	0.664	1.909	11.4	2.754	41.9	3.586	3.60	4.430	12.1	5.244	142	6.079	564	7.098	457
1.182	0.681	1.918	12.3	2.762	31.2	3.596	3.19	4.441	11.4	5.254	141	6.088	628	7.109	531
1.192	0.740	1.928	13.7	2.772	45.9	3.606	2.89	4.451	10.1	5.264	150	6.098	565	7.109	507
1.202	0.749	1.938	14.8	2.787	108	3.618	4.55	4.459	7.70	5.275	201	6.106	466	7.118	455
1.212	0.784	1.948	15.8	2.792	115	3.630	10.2	4.469	6.59	5.284	228	6.116	399	7.128	410
1.222	0.795	1.958	17.3	2.796	108	3.638	9.34	4.480	6.74	5.294	183	6.126	357	7.148	396
1.232	0.796	1.968	18.8	2.801	60.1	3.645	5.85	4.490	7.05	5.303	156	6.136	312	7.168	382
1.242	0.834	1.978	20.5	2.808	30.0	3.655	4.63	4.500	7.51	5.314	151	6.146	280	7.188	385
1.251	0.868	1.988	22.6	2.818	22.6	3.666	4.31	4.510	7.99	5.324	152	6.157	268	7.207	373
1.261	0.869	1.998	24.6	2.830	19.7	3.677	4.97	4.521	10.1	5.333	158	6.167	259	7.227	369
1.271	0.866	2.009	28.0	2.841	18.0	3.691	19.1	4.531	10.9	5.343	168	6.177	263	7.247	374
1.281	0.931	2.019	30.6	2.851	17.1	3.699	33.3	4.541	17.1	5.353	178	6.187	258	7.267	376
1.291	0.887	2.028	33.6	2.862	16.7	3.706	19.4	4.549	55.1	5.363	193	6.197	266	7.287	381
1.301	0.941	2.038	37.0	2.872	16.5	3.713	7.44	4.554	80.7	5.373	211	6.207	267	7.307	411

Continued on next page

TABLE I: – continued from previous page

E_{eff}	σ	E_{eff}	σ	E_{eff}	σ	E_{eff}	σ	E_{eff}	σ	E_{eff}	σ	E_{eff}	σ	E_{eff}	σ
(MeV)	(mb)	(MeV)	(mb)	(MeV)	(mb)	(MeV)	(mb)	(MeV)	(mb)	(MeV)	(mb)	(MeV)	(mb)	(MeV)	(mb)
1.303	0.918	2.048	40.3	2.882	16.5	3.722	4.16	4.558	89.6	5.383	225	6.216	271	7.326	438
1.305	0.930	2.057	43.1	2.892	17.0	3.733	2.75	4.561	76.2	5.393	238	6.226	266	7.346	441
1.307	0.950	2.067	44.2	2.902	17.0	3.744	2.31	4.564	57.7	5.403	243	6.236	265	7.366	454
1.309	0.958	2.077	44.5	2.911	17.3	3.755	2.03	4.568	45.0	5.413	240	6.246	260	7.386	445
1.311	0.990	2.087	48.5	2.921	17.6	3.765	1.72	4.578	37.1	5.423	237	6.256	267	7.406	456
1.333	2.21	2.097	45.2	2.931	18.1	3.775	1.60	4.588	27.4	5.433	235	6.266	274	7.427	484
1.334	4.26	2.106	41.2	2.941	18.7	3.786	1.53	4.598	21.6	5.443	240	6.276	284	7.445	502
1.335	10.8	2.116	39.5	2.951	19.8	3.795	1.50	4.609	20.1	5.452	251	6.286	301	7.465	500
1.336	48.2	2.126	38.2	2.962	21.1	3.805	1.47	4.619	20.2	5.462	254	6.296	314	7.485	509
1.337	10.9	2.136	37.4	2.972	22.1	3.815	1.42	4.629	21.0	5.472	240	6.306	326	7.505	498
1.338	4.27	2.146	37.5	2.982	24.4	3.825	1.39	4.639	22.5	5.482	202	6.316	349	7.525	498
1.339	2.22	2.156	39.8	2.992	27.6	3.835	1.36	4.649	24.2	5.492	173	6.325	356	7.544	491
1.365	1.14	2.167	42.8	3.002	31.9	3.845	1.39	4.659	25.9	5.502	151	6.335	362	7.564	450
1.377	1.13	2.177	47.0	3.012	37.3	3.855	1.37	4.670	28.1	5.512	135	6.345	358	7.584	431
1.389	1.12	2.187	53.0	3.021	41.6	3.865	1.43	4.679	29.3	5.522	123	6.355	344	7.605	430
1.400	1.09	2.197	59.9	3.031	45.8	3.875	1.47	4.688	29.9	5.532	114	6.365	337	7.625	452
1.410	1.11	2.207	66.4	3.041	47.6	3.885	1.57	4.698	30.3	5.542	107	6.375	322	7.645	499
1.420	1.16	2.217	75.2	3.051	46.1	3.895	1.71	4.708	29.8	5.552	101	6.385	308	7.664	555
1.431	1.21	2.227	75.3	3.060	43.8	3.905	1.84	4.718	30.0	5.561	96.6	6.395	296	7.684	613
1.441	1.19	2.236	74.1	3.070	41.2	3.915	2.01	4.728	29.8	5.571	94.1	6.405	273	7.704	680
1.450	1.22	2.245	73.3	3.080	38.8	3.925	2.28	4.738	29.6	5.581	92.0	6.415	261	7.724	691
1.461	1.29	2.255	67.7	3.090	37.4	3.935	2.61	4.748	30.1	5.591	91.1	6.425	255	7.744	664
1.471	1.29	2.265	66.2	3.100	37.3	3.945	2.95	4.758	30.6	5.601	91.3	6.435	246	7.763	638
1.480	1.31	2.275	59.1	3.111	36.9	3.955	3.43	4.768	31.0	5.611	91.8	6.444	243	7.783	614
1.490	1.31	2.285	56.0	3.121	37.0	3.965	4.07	4.778	31.3	5.621	94.0	6.454	244	7.803	592
1.500	1.37	2.295	55.1	3.130	37.9	3.975	4.62	4.787	29.8	5.631	97.3	6.464	246	7.823	596

Continued on next page

TABLE I: – continued from previous page

E_{eff}	σ	E_{eff}	σ	E_{eff}	σ	E_{eff}	σ	E_{eff}	σ	E_{eff}	σ	E_{eff}	σ	E_{eff}	σ
(MeV)	(mb)	(MeV)	(mb)	(MeV)	(mb)	(MeV)	(mb)	(MeV)	(mb)	(MeV)	(mb)	(MeV)	(mb)	(MeV)	(mb)
1.510	1.42	2.305	53.8	3.140	39.2	3.985	5.14	4.797	29.0	5.641	100	6.474	245	7.843	595
1.520	1.44	2.315	53.7	3.150	40.4	3.995	5.62	4.807	27.0	5.651	107	6.484	240	7.863	599
1.530	1.57	2.325	52.9	3.160	42.3	4.005	6.20	4.817	25.5	5.662	115	6.494	241	7.882	622
1.541	1.67	2.335	54.3	3.170	44.4	4.014	6.55	4.827	24.9	5.671	127	6.504	243	7.902	640
1.550	1.62	2.346	56.5	3.180	47.2	4.024	7.05	4.837	24.8	5.681	142	6.514	244	7.922	583
1.560	1.75	2.355	59.0	3.190	52.4	4.034	7.59	4.848	25.8	5.691	163	6.524	245	7.941	501
1.585	2.90	2.365	63.3	3.200	56.9	4.044	8.83	4.858	27.2	5.701	182	6.534	244	7.962	458
1.587	3.20	2.375	66.4	3.210	61.2	4.055	12.5	4.868	29.6	5.711	204	6.544	240		